Modeling of Aircraft Measurements of Ice Crystal Concentration in the Arctic and a Parameterization for Mixed-Phase Cloud

SONGMIAO FAN

NOAA/Geophysical Fluid Dynamics Laboratory, Princeton, New Jersey

DANIEL A. KNOPF

Institute for Terrestrial and Planetary Atmospheres, School of Marine and Atmospheric Sciences, Stony Brook University, State University of New York, Stony Brook, New York

ANDREW J. HEYMSFIELD

National Center for Atmospheric Research, Boulder, Colorado

LEO J. DONNER

NOAA/Geophysical Fluid Dynamics Laboratory, Princeton, New Jersey

(Manuscript received 8 February 2017, in final form 5 September 2017)

ABSTRACT

In this study, two parameterizations of ice nucleation rate on dust particles are used in a parcel model to simulate aircraft measurements of ice crystal number concentration N_i in the Arctic. The parcel model has detailed microphysics for droplet and ice nucleation, growth, and evaporation with prescribed vertical air velocities. Three dynamic regimes are considered, including large-scale ascent, cloud-top generating cells, and their combination. With observed meteorological conditions and aerosol concentrations, the parcel model predicts the number concentrations of size-resolved ice crystals, which may be compared to aircraft measurements. Model results show rapid changes with height/time in relative humidity, N_i, and thermodynamic phase partitioning, which is not resolved in current climate and weather forecasting models. Parameterizations for ice number and nucleation rate in mixed-phase stratus clouds are thus developed based on the parcel model results to represent the time-integrated effect of some microphysical processes in large-scale models.

1. Introduction

Mixed-phase clouds, comprising both ice and supercooled liquid water, are frequently observed in the Arctic (Shupe et al. 2006; Verlinde et al. 2007; de Boer et al. 2011; Shupe 2011; Morrison et al. 2012). The thermodynamic phase partitioning in clouds is influenced locally by heterogeneous ice nucleation rates and the Wegener–Bergeron–Findeisen (WBF) process, which involves the growth of ice crystals via vapor deposition and evaporation of liquid water droplets (e.g., Rotstayn et al. 2000) and influences the equilibrium climate sensitivity to atmospheric CO_2 concentration (Tan et al. 2016). The rate of the WBF process increases with the concentration of ice crystals in clouds, which itself increases with the number of ice nucleating particles (INPs). Atmospheric insoluble aerosols can serve as INPs as air cools to critical temperatures T and reaches critical ice supersaturations (SSi) [see, e.g., review by Hoose and Möhler (2012)]. Model prediction of the mixed-phase clouds thus requires accurate representation of atmospheric aerosols such as cloud condensation nuclei (CCN), a variety of INPs and their concentrations, the WBF process, large-scale synoptic meteorological processes, and small-scale dynamics that drive microphysical processes. The concentration of ice crystals is an observable parameter linking ice nucleation and subsequent microphysical processes in clouds that could not be readily measured in situ, as long as the ice crystal concentration can be reliably measured.

Corresponding author: Songmiao Fan, songmiao.fan@noaa.gov

DOI: 10.1175/JAS-D-17-0037.1

TABLE 1. Aircraft measurements of ice crystal number concentrations in the Arctic. Some data are for single cloud and others are for averages of many clouds.

Field campaign and location	Month and year	Reference	Base Z (m)	Top Z (m)	Base T (K)	Top T (K)	Ice crystal N_i (L^{-1})	Size D (μm)
BASE; Beaufort Sea	Sep and Oct 1994	Pinto et al. (2001)	5300	5800	—	240	77.6	>50
			<4300	6200	—	239	33.7	
			Mixed-phase clouds (see Fig. 9)				2.8 (0.01–12.3)	>50
SHEBA; Chukchi Sea	May and Jun 1998	Rangno and Hobbs (2001)	Mixed-phase clouds (see Fig. 9, with data from BASE)					
FIRE-ACE; Northwest Territories	Apr 1998	Gultepe et al. (2001)	Glaciated clouds (see Fig. 10, with data from BASE)					
M-PACE; Alaska	Oct 2004	McFarquhar et al. (2007)	542	1238	263	258	5.62 ± 12.10	>53
			583	1154	262	258	1.60 ± 2.40	
			745	1322	260	257	2.04 ± 2.06	
			420	885	262	261	2.07 ± 4.97	
Indirect and Semi-Direct Aerosol Campaign (ISDAC); Alaska	Apr 2008	Avramov et al. (2011)	500	1000	—	259	0.5 ± 0.2	>100
Aerosol-Cloud Coupling And Climate Interactions in the Arctic (ACCACIA); Svalbard	Mar and Apr 2012	Lloyd et al. (2015)	1200	1700	—	254	0.61	—
			900	1400	—	256	0.47	

Aircraft measurements of ice crystals have been made in Arctic clouds during multiple field expeditions (Table 1). The number concentrations of ice crystal were found mostly in the range of 0.1–100 L^{-1} at standard conditions (T = 273.2 K; pressure P = 1013 hPa), which is three to six orders of magnitude lower than that of liquid droplets (Gultepe et al. 2001; Pinto et al. 2001; McFarquhar et al. 2007; Avramov et al. 2011; Lloyd et al. 2015). Most of the ice crystals were between 50 and 200 μm in diameter, and their habits were recognized as needles, dendrites, rosettes, semispheres, or irregular in shape (McFarquhar et al. 2007; Avramov et al. 2011). Measurements of ice smaller than 50 μm were subject to interference from shattering at air-sampling inlets and other measurement uncertainties (McFarquhar et al. 2011). Larger frozen hydrometeors were observed below the liquid cloud layer with number concentrations on the order of 1 L^{-1}, indicating a continual settling of ice from above. The dominant particle types identified as INPs in the Arctic were mineral dust/metal oxides, carbonaceous particles, and mixtures of metal oxides/dust with either carbonaceous components or salts/sulfates (Prenni et al. 2009; McFarquhar et al. 2011).

Over the Arctic Ocean, the formation of mid- and upper-level clouds is believed to be closely associated with frontal systems (Curry and Herman 1985). Low-level clouds appear to be relatively insensitive to the synoptic situation and form as a result of airmass modification due to radiative cooling (Curry et al. 1996). Cloud-top cooling and in-cloud latent heating act to maintain Arctic mixed-phase stratocumulus in the presence of a temperature and humidity inversion for many days at a time (Solomon et al. 2011). Deep convection may occur over ice-free ocean (Noer et al. 2011). More complex cloud processes, including that of multilayer clouds, result from cloud, radiation, moisture, and dynamical interactions (Curry et al. 1996; Morrison et al. 2012). The role of aerosols and INPs in the persistence of Arctic mixed-phase clouds could be important and needs further investigation (Morrison et al. 2012).

Some climate models and forecast models are deficient in simulating liquid-containing Arctic clouds with substantial consequences on surface radiation (Xie et al. 2008; Liu et al. 2011; Cesana et al. 2012; Sotiropoulou et al. 2016; Tan et al. 2016). Cloud-resolving models and single-column models also have difficulties reproducing the observed cloud fields in observationally based case studies (Klein et al. 2009; Morrison et al. 2009). The primary culprit in the underestimation of liquid water content (LWC) in these models is the treatment of the WBF process, which is sensitive to N_i and thus to the concentration of INPs (e.g., Jiang et al. 2000; Fan et al. 2011; Tan et al. 2016). Previous parameterizations for INPs range from simple empirical relationships with T (Fletcher 1962), SSi (Meyers et al. 1992), and T and aerosol (Phillips et al. 2008; DeMott et al. 2010; Niemand et al. 2012; Phillips et al. 2013; DeMott et al. 2015) to more comprehensive relationships with vertical velocity w, T, SSi, and aerosol concentrations (Khvorostyanov and Curry 2004; Liu and Penner 2005; Barahona et al. 2010).

Laboratory experiments have been conducted to study ice nucleation in the deposition and the condensation–immersion modes for multiple INPs including dust

particles of different mineralogical compositions, soot and organic particles, and primary biological particles (Hoose and Möhler 2012; Murray et al. 2012). In these experiments, the activated fraction was measured as a function of T and SSi. The measurements were interpreted with a stochastic freezing model based on the classical nucleation theory (CNT) and/or with the singular freezing model. In the CNT, the rates of nucleation are characterized by different contact angles θ and activation energies $\Delta g^{\#}$ for different INPs (Chen et al. 2008; Hoose et al. 2010) or by different relationships between θ and T (Zobrist et al. 2007). In the singular freezing model, the number of active sites per surface area is characterized as a function of T for each type of INP (Hoose and Möhler 2012; Niemand et al. 2012). A key difference between the stochastic and singular models is that the latter neglects ice nucleation kinetics (Alpert and Knopf 2016). In other words, the stochastic approach accounts for the effects of T and time while the singular description accounts for T only. A continued immersion freezing could sustain the formation of ice and steady precipitation of ice observed in long-lived supercooled-layer clouds (de Boer et al. 2010; Westbrook and Illingworth 2013). By contrast, if activated rapidly as assumed in the singular description, available INPs are depleted from a mixed-phase boundary layer cloud within minutes (Fridlind et al. 2012).

A relationship between the nucleation rate coefficient per unit INP surface area $J_{\rm het}$ ($\rm m^{-2}\,s^{-1}$) and water activity a_w [approximately the same as ambient relative humidity (RH) in fraction when droplet and surrounding water vapor are in equilibrium] has been proposed recently for immersion freezing (Knopf and Alpert 2013; Alpert and Knopf 2016). In the a_w-based immersion freezing model (ABIFM), $J_{\rm het}$ is calculated according to

$$\log_{10}(J_{\rm het}) = m[a_w(T) - a_{w,\rm ice}(T)] + c, \quad (1)$$

$$a_{w,\rm ice}(T) = p_{\rm ice}(T)/p_w(T), \quad (2)$$

where $p_{\rm ice}(T)$ and $p_w(T)$ are the saturation water vapor pressure of ice and pure liquid water at temperature T. The values of $a_{w,\rm ice}$ at T can be computed with high accuracy (Koop and Zobrist 2009). The parameters, c and m, were estimated for each type of INP based on laboratory nucleation experiments (Knopf and Alpert 2013; Alpert and Knopf 2016).

In this study, the parameters (θ, $\Delta g^{\#}$, c, and m) obtained from fitting laboratory measurements are used to predict ice nucleation on dust aerosols in a parcel model. The results are compared to aircraft measurements of N_i in the Arctic troposphere and elsewhere, which highlights the need for more targeted concurrent observations of clouds, dynamics, and INP. Our objectives are threefold: 1) to assess which parameter sets yield better agreements with the aircraft data; 2) to obtain familiarity with the time evolution of N_i, SSi, water supersaturation (SSw), ice–liquid partition, size distribution of hydrometeors, and their dependence on w and aerosols; and 3) to derive new parameterizations for ice nucleation, which account for the effect of rapidly changing RH (i.e., SSi and SSw) and allow for sub-grid-scale variation of the thermodynamic phase partitioning.

The remainder of the papers is laid out as follows. The parcel model and simulations are described in section 2. Model results for stratocumulus simulations and for stratus are presented in sections 3 and section 4, respectively. New parameterizations are presented in section 5. Parcel model results are compared to aircraft measurements of N_i over the Arctic in section 6. A summary of results and conclusions are given in section 7.

2. Model description

An adiabatic parcel model calculates pressure P and temperature T as air moves up or down from an initial state while the parcel has no exchange of mass or energy with its environment. It prescribes dynamic forcing through vertical velocity w and neglects the thermodynamic effects of radiative heating/cooling and entrainment, both of which occur in the atmosphere. The parcel model is thus an approximation of the changing state (i.e., P and T), which is suitable for simulating cloud microphysical processes occurring on relatively short time scales under the restricted conditions. The model predicts SSi, SSw, and droplet and ice crystal number concentrations and sizes. The equations for time rate of change is integrated forward in time at a 0.1-s time step, except for INP and N_i increments, which are calculated at 20-s time step.

In the parcel model, droplets form when diffusion of water molecules to deliquescent aerosols cause rapid growth as a critical supersaturation over water is reached (Pruppacher and Klett 1997). The rate of homogeneous ice nucleation is calculated in deliquescent sulfate and sea salt aerosols and in liquid water droplets (Koop et al. 2000). The rate of heterogeneous ice nucleation is calculated in dust and soot aerosols as the sum of rates in the deposition mode and in the condensation–immersion mode. Contact nucleation is limited by drop–INP collision and is neglected in this study. The rate of deposition freezing is calculated based on the CNT (Chen et al. 2008; Hoose et al. 2010).

TABLE 2. Condensation–immersion freezing parameters.

Parameterization	Dust and experiment	Mode of nucleation	Parameters
Chen et al. (2008); Hoose et al. (2010)	Illite (Zimmermann et al. 2008)	Deposition	$\theta = 12.7°$, $\Delta g^{\#} = -6.21 \times 10^{-21}$ J
Knopf and Alpert (2013); Alpert and Knopf (2016)	Natural dust particles (Niemand et al. 2012)	Condensation or immersion freezing	$c = -1.35$, $m = 22.62$

The rate of immersion freezing is calculated based on the ABIFM (Knopf and Alpert 2013; Alpert and Knopf 2016). The parameters used in the parcel model are listed in Table 2.

Growth of ice crystals occurs by molecular diffusion (Pruppacher and Klett 1997) and is calculated with habit evolution based on the two-axis oblate or prolate spheroid method (Sulia and Harrington 2011). Ice larger than 200 μm in diameter D (for a mass equivalent sphere) is excluded from further growth or sublimation to indicate that they have settled out of the air parcel. This choice of critical size is guided by previous studies (Morrison and Gettelman 2008). It is noted that ice crystals larger than 200 μm are often observed in mixed-phase clouds (Heymsfield et al. 2013; Yang et al. 2013, 2014). Increasing the critical size, allowing accumulation and continued growth of larger ice crystals by vapor deposition, would cause more dehydration and more rapid evaporation of droplets (Fan 2013). The concentration of these "snow" particles N_s increases monotonically in the model. Evaporation of droplets and sublimation of ice occur when the air becomes subsaturated. Collision and accretion of hydrometeors are not considered. The parcel model also neglects ice multiplication by the Hallett–Mossop process, which is important between 265 and 270 K (Hallett and Mossop 1974; Rangno and Hobbs 2001), or by shattering of freezing drops, which may be important when the drops are large (Rangno 2008; Gayet et al. 2009; Lawson et al. 2015).

The size distribution of dry aerosols is assumed to be lognormal and is discretized into 20 logarithmically equal size bins between 0.01 and 10 μm in radius. A single-modal distribution is specified for sulfate, sea salt, and soot aerosols, and a two-modal distribution is specified for dust aerosols (Fan 2013). Dust and soot aerosols are assumed to be an insoluble spherical core with sulfate coating (5% by mass for dust and 50% for soot). These specifications are the same for all simulations.

Four sets of simulations were conducted in this study (Table 3). In S1, the parcel oscillates within a 550-m horizontal layer with vertical velocities varying linearly with height increasing from 0.04 m s^{-1} at the base to a maximum of 0.5 m s^{-1} at 275 m and decreasing to 0.04 m s^{-1} at the top, then with w in reversed sign from the top to the base, in order to simulate stratocumulus in the Arctic boundary layer (Solomon et al. 2011). In S2, the parcel ascends at a constant w (0.1, 0.3, 0.5, and 1.0 m s^{-1}) to simulate stratus associated with large-scale isentropic advection. In S3, the parcel oscillates in a 550-m slanted layer (i.e., the combination of S1 and S2 at $w = 0.1$ m s^{-1}) to simulate cloud-top generating cells embedded in a large-scale stratus. Deposition freezing is set to zero in S1–S3. In S4, the parcel moves as in S2, but deposition freezing is initiated at about 15% ice supersaturation. Soluble coating is assumed to inhibit deposition nucleation in S1–S3 and to have no impact in S4. Initial aerosol concentrations, P, and T for the simulations are also shown in Table 3. Dust concentrations are specified to between 0.05 and 10 μg m^{-3} in separate simulations to show the sensitivity of N_i to INP concentration, covering the range of observations of dust in the Arctic (McNaughton et al. 2011; Fan 2013; Breider et al. 2014; Zwaaftink et al. 2016). Soot concentration is set to zero because of uncertainty on whether soot aerosols act as ice nuclei at T warmer

TABLE 3. Model simulations. Deposition nucleation is set to zero for the S1–S3 series assuming coated dust particles do not initiate ice nucleation in this mode, and it is calculated in S4 regardless of coating.

Simulation	Initial P (hPa)	Initial T (K)	w (m s^{-1})	Dust (μg m^{-3})
S1 series	950	244–268	−0.5 to 0.5	0.5, 2.0
S2 series	950	244–268	0.03, 0.1, 0.3, 0.5, 1.0	0.05, 0.5, 2.0, 10
	475	244–268	0.03, 0.1, 0.3, 0.5, 1.0	2.0
	850, 750, 650, 550	244–268	0.1	2.0
S3 series	950	244–268	0.1 + (−0.5 to 0.5)	0.5, 2.0
S4 series	950	244–268	0.03, 0.1, 0.3, 0.5, 1.0	0.05, 0.5, 2.0, 10

than 240 K (Friedman et al. 2011). Sulfate and sea salt are both specified to be 1 μg m^{-3} in concentration.

3. Ice in stratocumulus

Parcel model simulations were carried out for stratocumulus with initial T between 244 and 268 K (S1 in Table 3). Here, we show some model results for two initial T values as examples. Figure 1 shows the time profiles of variables predicted in the model for an initial T of 262 K and a dust concentration of 0.5 μg m^{-3} (~1.4 particles per cubic centimeter; ~0.17 cm^{-3} with $D > 0.5\,\mu$m). As the parcel oscillates in the layer, air T also oscillates between 262 and 257 K (Fig. 1a). The air becomes supersaturated over water at ~150 m on ascent (Fig. 1b) and then droplet activation occurs. The number of droplets N_d increases quickly from 0 to ~120 cm^{-3} while the LWC increases from 0 at cloud base to ~0.25 g kg^{-1} at cloud top (Fig. 1c). Ice nucleation in the immersion mode is initiated before droplet activation, but the rate is slower below water saturation than at saturation (Fig. 1d). Ice supersaturation increases rapidly when N_i ($D < 200\,\mu$m) is small and more slowly when N_i is greater (Figs. 1b and 1d). The decrease of N_i on descent is due to a combination of zero or slower ice nucleation and conversion to snow ($D = 200\,\mu$m) by depositional growth (Fig. 1d). Over four ascent–descent cycles, a total of 5 L^{-1} ice crystals are produced ($N_i + N_s$ in Fig. 1d) while N_i fluctuates between ~0.1 and 0.5 L^{-1} during this period. All these results are in good agreement with aircraft measurements, which include ice particles smaller than 200 μm (N_i) and larger ones (remaining fraction of N_s) (McFarquhar et al. 2007; Avramov et al. 2011). The observations of ice crystals in the Arctic stratocumulus clouds have a median value of ~0.5 L^{-1} in March and April and 2–5 L^{-1} in October (Table 1). More INPs in October may originate from ice-free ocean (Knopf et al. 2011; Alpert et al. 2011; Yun and Penner 2013; DeMott et al. 2016; Wilson et al. 2015), terrestrial vegetation (Tobo et al. 2013), and high-latitude sources of dust (Barrie and Barrie 1990; Crusius et al. 2011; Bullard et al. 2016; Zwaaftink et al. 2016).

Figure 2 shows the time profiles of variables predicted in the model for an initial T of 253 K. At the low temperatures (Fig. 2a), rapid ice nucleation produces large N_i (Fig. 2d) and causes dehydration (Fig. 2b). Droplet activation occurs in the first two ascent–descent cycles but not later, indicating that stratocumulus is not sustainable at the lower temperatures because the air is being dehydrated to prevent the formation of liquid water, which is required to generate sufficient cloud-top radiative cooling and downdraft (Solomon et al. 2011).

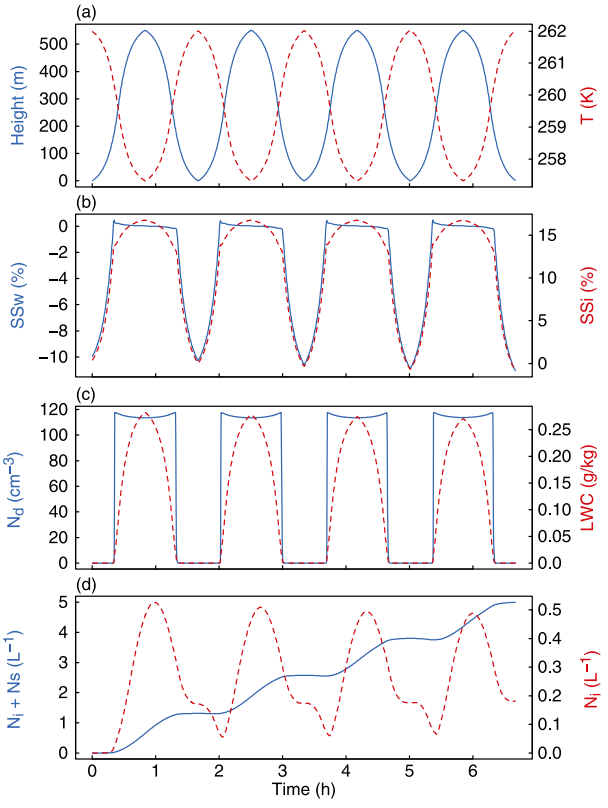

FIG. 1. A parcel model simulation of a stratocumulus cloud (S1 in Table 3). Model results are given as a function of time for [dust] = 0.5 μg m^{-3}, w oscillating between −0.5 and 0.5 m s^{-1}, initial P = 950 hPa, and initial T = 262 K. (a) Height (left axis, solid) and T (right axis, dashed), (b) SSw (left axis, solid) and SSi (right axis, dashed), (c) N_d (left axis, solid) and LWC (right axis, dashed), and (d) sum of ice N_i and snow N_s (left axis, solid) and N_i (right axis, dashed).

The value of N_i is proportional to INP concentration in mixed-phase clouds in which ice nucleation is not self-limited by low RH or dehydration. A large number of INPs cause a large N_i and more rapid vapor deposition on ice, which may inhibit the formation of stratocumulus. When the INP concentration is low, the mixed-phase stratocumulus may be maintained at very low temperatures, as often observed in the Arctic.

4. Ice in stratus

Parcel model simulations were also carried out for stratus with initial temperatures between 244 and 268 K, dust concentrations from 0.05 to 10 μg m^{-3}, and a range of vertical velocities (S2 in Table 3). In this section, we show some model results for two updraft velocities as examples. In the next two sections, we construct parameterizations for ice in mixed-phase clouds based on these simulations and compare parcel

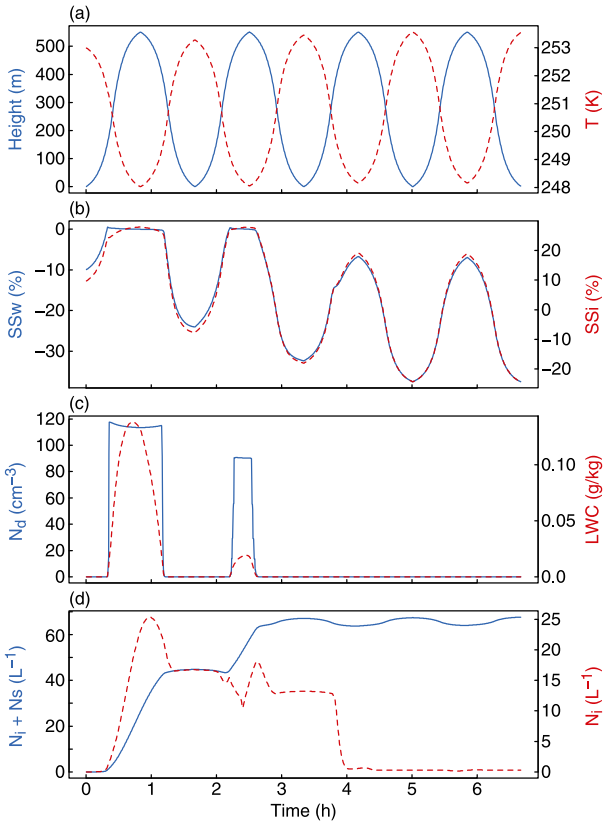

FIG. 2. As in Fig. 1, but for initial $T = 253$ K.

model results of N_i in stratus to aircraft measurements, respectively.

Figure 3 shows model results for $w = 0.1\,\mathrm{m\,s^{-1}}$ and a dust concentration of $0.5\,\mu\mathrm{g\,m^{-3}}$ in the first 600 m. Results from higher altitudes are not shown because they are to a large extent represented by simulations for lower initial temperatures. At low temperatures, fast ice nucleation results in large N_i, which causes rapid decreases in SSw (Fig. 3a) and SSi (Fig. 3b). At the lowest T values, ice nucleation is fast enough to dehydrate the air and prevent droplet activation (Fig. 3a). The decrease of N_i after a peak concentration is again due to a combination of slowdown or cessation of ice nucleation, caused by decreases of RH, and conversion to snow (Fig. 3c). It takes about 1000 s to grow a newly formed ice crystal to 200 μm in diameter (Yang et al. 2013). For comparison, we estimated a residence time of ~1300 s for ice crystals in a long-lived supercooled cloud layer based on the observed ice number concentrations in the column, and a steady flux of ice crystals fell from the cloud (Westbrook and Illingworth 2013). At warmer temperatures, N_i continues to increase with height as air temperature decreases (Fig. 3d), which indicates the rate of nucleation is greater than conversion to snow.

Model results for $w = 1\,\mathrm{m\,s^{-1}}$ and a dust concentration $0.5\,\mu\mathrm{g\,m^{-3}}$ are shown in Fig. 4. As the parcel ascends more rapidly, water supersaturation is reached for all initial temperatures (Fig. 4a). SSi continues to increase but at slower rates after the initiation of ice (Fig. 4b). At low temperatures, more ice is nucleated for $w = 1\,\mathrm{m\,s^{-1}}$ than for $w = 0.1\,\mathrm{m\,s^{-1}}$ (cf. Figs. 3c and 4c), because more rapid immersion nucleation occurs in a liquid droplet than in a deliquescent aerosol with the same insoluble core. At warmer temperatures, however, a factor-of-4 fewer ice crystals are nucleated for $w = 1\,\mathrm{m\,s^{-1}}$ than for $w = 0.1\,\mathrm{m\,s^{-1}}$ (cf. Figs. 3d and 4d). This is because ice nucleation occurs at the same rates (at the same temperature and at water saturation), but the 10-times-longer period to reach 600 m for the case of $w = 0.1\,\mathrm{m\,s^{-1}}$ allows more conversion to snow as well as 10 times more ice nucleation, which have partially compensating effects on N_i (i.e., reduction from 10 to 4 times).

Our simulations (S3) for stratus with cloud-top generating cells yield results (not shown) more similar to the simulations for stratus than for stratocumulus. This indicates the dominant effect of the large-scale ascent ($w = 0.1\,\mathrm{m\,s^{-1}}$) on P, T, and RH over that of the small-scale vertical motions embedded within. The effect of vertical oscillation w' is minor because the probability distribution of w' is close to a Gaussian distribution: most of the time, $|w'|$ is $<0.1\,\mathrm{m\,s^{-1}}$ and w' at the tails of the distribution occurs in short periods. The effect of w' is relatively more important if the large-scale w is smaller. It should be noted that these simulations do not apply to more vigorous convective cells occurring above stratus associated with midlatitude synoptic systems or in cirrus associated with convective outflows.

5. Parameterizations for ice in mixed-phase clouds

The above results demonstrate the intricate time and height patterns of N_i, SSi, and SSw as they are associated with w and T. The concentration of INP is another important factor influencing the microphysics in mixed-phase clouds. The rapid changes with height and time found in the parcel model simulations are not resolved in atmospheric models with large model time steps. Parameterizations must be developed to represent ice nucleation and the WBF process in the large-scale models. In this section, we construct a parameterization for N_i as a function of w, T, and dust concentrations for stratus clouds, which is appropriate for use with the WBF scheme derived by Rotstayn et al. (2000). We also construct a parameterization for the rate of N_i source as a function of w, T, and dust, which is appropriate for use with the WBF scheme adopted by

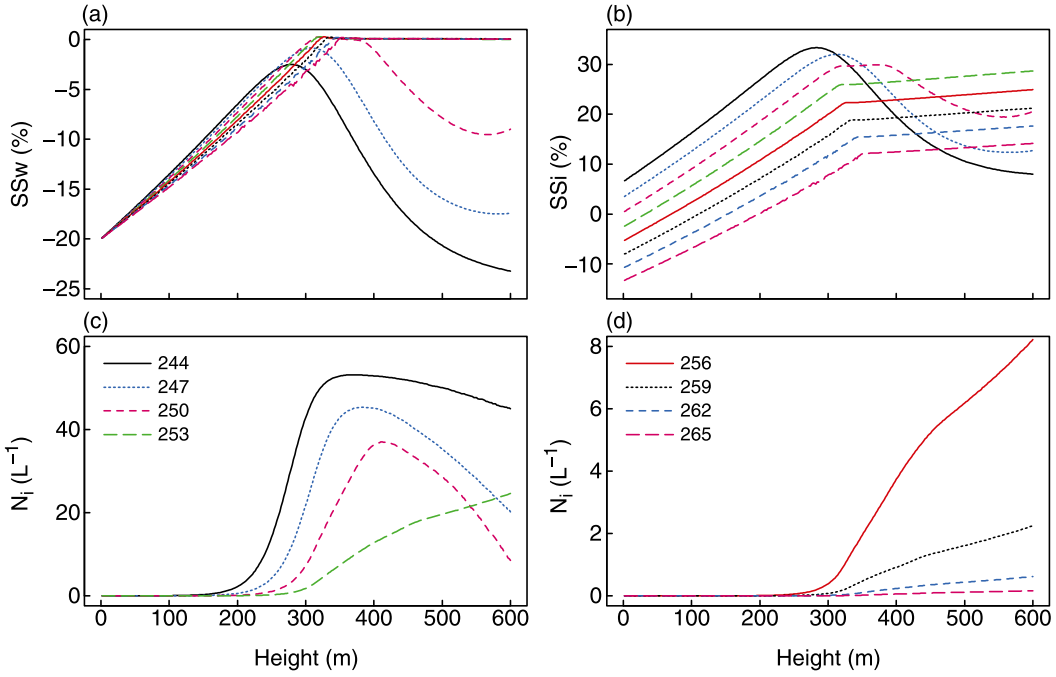

FIG. 3. A parcel model simulation of a stratus cloud (S2 in Table 3). Model results are given as a function of height for [dust] = 0.5 μg m^{-3}, w = 0.1 m s^{-1}, initial P = 950 hPa, and variable initial T (see legend for lines). (a) SSw, (b) SSi, (c) N_i (T = 244, 247, 250, and 253 K), and (d) N_i (T = 256, 259, 262, and 265 K). Legends for lines in (c) and (d) also apply for lines in (a) and (b), respectively.

Morrison and Gettelman (2008). The new parameterizations will be compared to some existing parameterizations that are used for stratus in climate models. A parameterization for stratocumulus will be developed based on additional simulations similar to S1 (Table 3) for a range of vertical velocity profiles and cloud thicknesses, to be reported in a forthcoming paper. A parameterization for convective clouds needs to consider

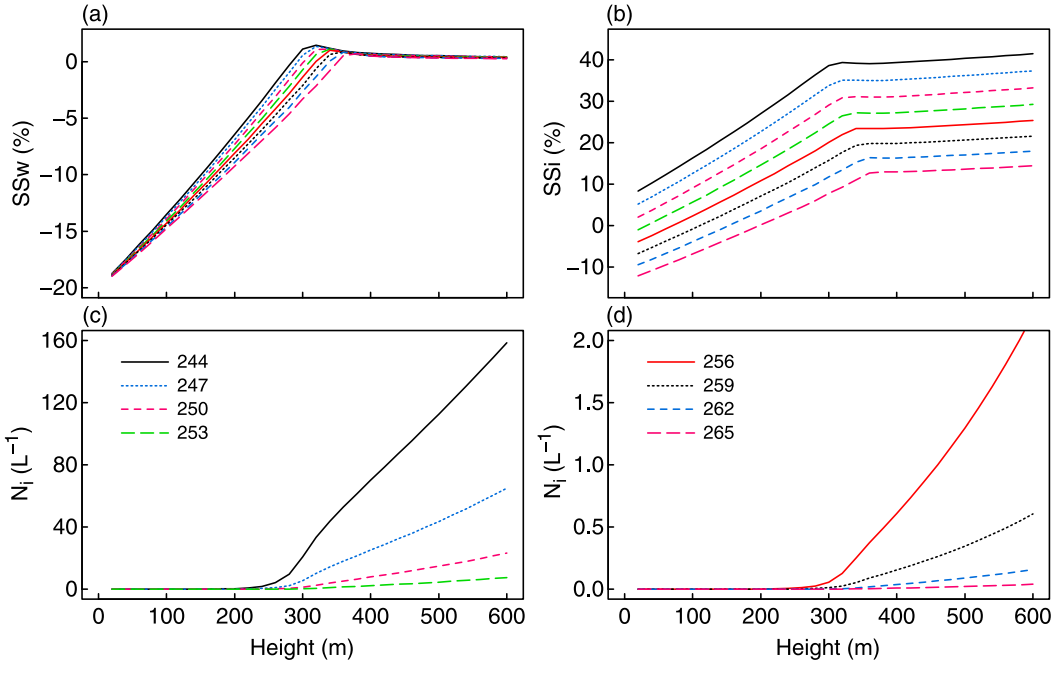

FIG. 4. As in Fig. 3, but for w = 1.0 m s^{-1}.

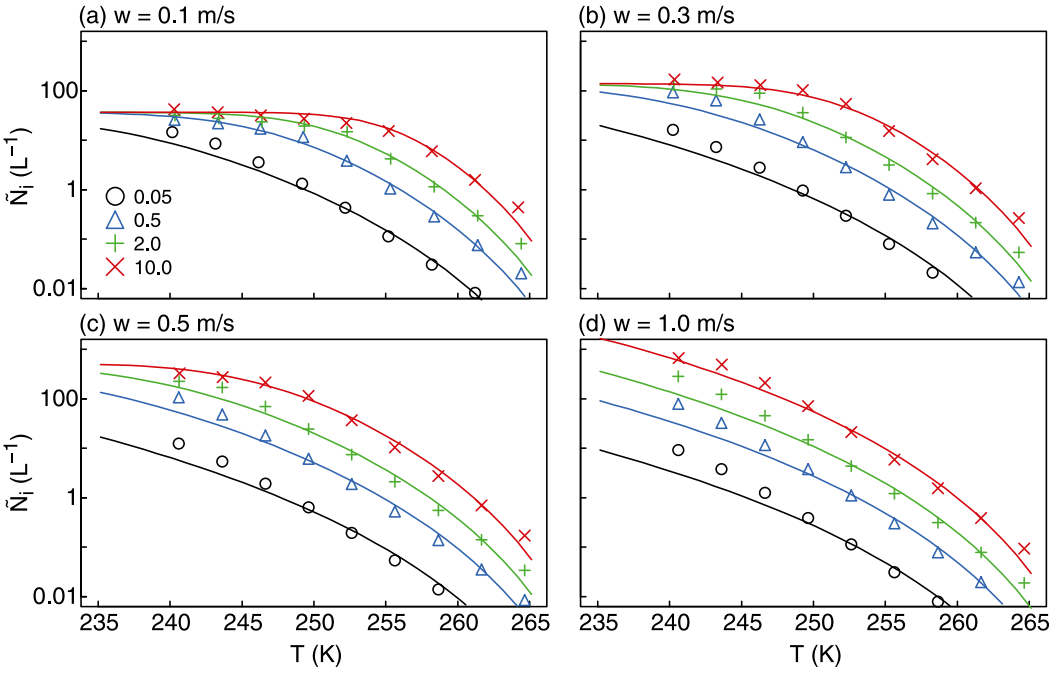

FIG. 5. Number concentration of ice crystals $\tilde{N}_i$ as a function of T for w = (a) 0.1, (b) 0.3, (c) 0.5, and (d) 1.0 m s^{-1}. Symbols indicate model output, and lines indicate calculations based on Eqs. (3) and (4). Colors indicate dust concentrations: 0.05 (black), 0.5 (blue), 2.0 (green), and 10 μg m^{-3} (red).

entrainment, ice multiplication, and large vertical velocities and is beyond the scope of this study.

In the WBF scheme of Rotstayn et al. (2000), a liquid cloud is assumed initially and a constant number of ice crystals grow (from an initial size) at ice supersaturation, which may cause water subsaturation and thus the evaporation of liquid water. In effect, a steady-state N_i is assumed for the model time step. However, a steady-state N_i does not exist in most clouds as suggested by the parcel model results (Figs. 3 and 4). We choose to approximate this "steady state" N_i with 1/2 of the maximum N_i from 0 to 600 m $\tilde{N}_i$, which is effectively responsible for the WBF process within this column (Figs. 3 and 4). The choice of 600 m is based on considerations of typical thickness of stratiform mixed-phase clouds and climate model layers in the free troposphere. A relationship of $\tilde{N}_i$ with w, T, and dust concentration is then derived by a method of trial and error and least squares, where w and dust concentration are model inputs and T is the mean temperature from 200 to 600 m. The relationship is given by the following equations:

$$\tilde{N}_i = Ae^{\alpha w}[1 - \mathrm{sech}(x^3)], \tag{3}$$

$$x = Be^{\beta w}(273.16 - T)^{\gamma}(f_{\mathrm{act}}[\mathrm{dust}])^{1/6}, \tag{4}$$

where $\alpha = 6.65, \beta = -1.32, \gamma = 1.18, A = 18.8, B = 0.0277$, $f_{\mathrm{act}} = 1$, and [dust] indicates dust concentration. The factor f_{act} (see discussions below) is the active particle fraction and is intended to be a tunable parameter. Measurements show that f_{act} is dependent on T and mineralogical composition (Kaufmann et al. 2016). The inactive particles may yet initiate ice nucleation at lower temperatures or higher ice supersaturation than simulated in the parcel model (Hoose et al. 2010; Kanji and Abbatt 2010; Wang and Knopf 2011). In these equations, the unit for $\tilde{N}_i$ is per liter and for dust is micrograms per cubic meter (volume at P = 950 hPa and T). In Fig. 5, the parcel model results for $\tilde{N}_i$ (symbols) are compared with those calculated by the Eqs. (3) and (4) (lines). The lines generally follow the symbols as $\tilde{N}_i$ vary with T for different w and dust values, although the goodness of fit is not uniform with the lines deviating from the symbols at $T < 250$ K.

In the scheme of Morrison and Gettelman (2008), N_i is a prognostic variable for which a source ΔN_i is calculated every time step (or substep). For instance, ΔN_i may be calculated from the empirical relationship of Meyers et al. (1992) [Eq. (6a)] or DeMott et al. (2015) [Eq. (6b)] for condensation–immersion nucleation:

$$\Delta N_i = N_{\mathrm{INP}}(T + \Delta T) - N_{\mathrm{INP}}(T), \tag{5}$$

$$N_{\mathrm{INP}}(T) = \exp\{-0.639 + 0.1296 \times [\mathrm{RH}_i(T) - 100]\}, \tag{6a}$$

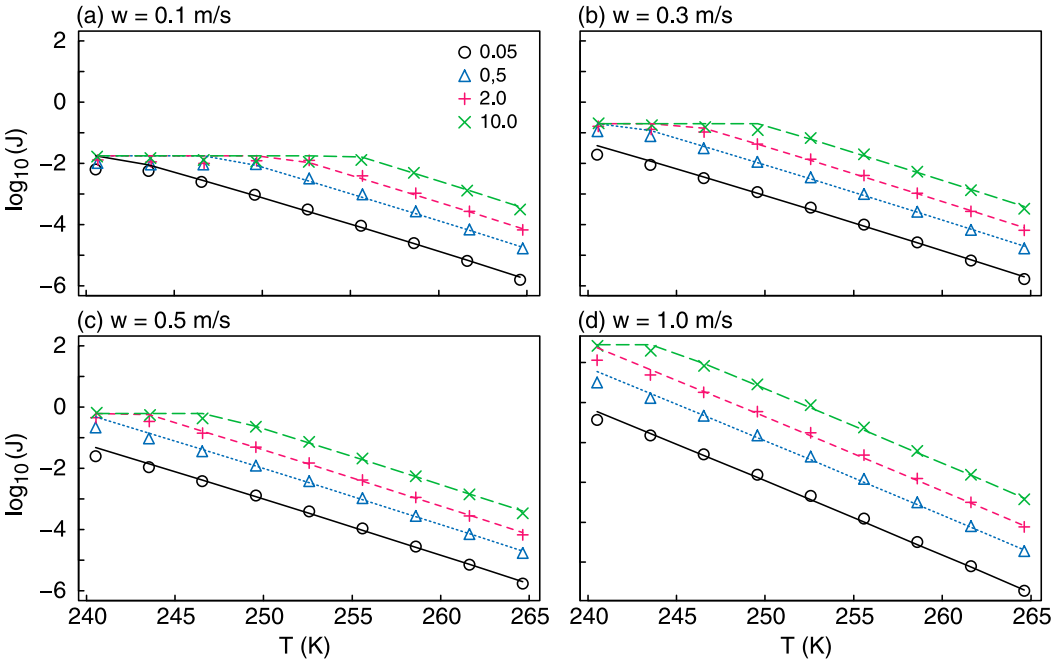

FIG. 6. The rate of ice nucleation J ($L^{-1}\,s^{-1}$, shown in $\log_{10}$) as a function of T for w = (a) 0.1, (b) 0.3, (c) 0.5, and (d) 1.0 m s^{-1}. Symbols indicate model output, and lines indicate calculations based on Eq. (8). Colors indicate dust concentrations: 0.05 (black), 0.5 (blue), 2.0 (green), and 10 μg m^{-3} (red).

$$N_{\mathrm{INP}}(T) = (\mathrm{cf})(n_{a>0.5\mu\mathrm{m}})^{1.25}\exp[0.46(273.16 - T) - 11.6], \tag{6b}$$

$$\Delta T = \frac{\partial T}{\partial z} w \Delta t, \tag{7}$$

where N_{INP} is the number concentration (standard: L^{-1}) of INPs, $\mathrm{RH}_i(T)$ is percentage relative humidity over ice at saturation vapor pressure over liquid water and dependent on T (K), cf is a calibration factor (=3), $n_{a>0.5\mu\mathrm{m}}$ is number concentration (standard: cm^{-3}) of dust particles larger than 0.5 μm in diameter, and ΔT and Δt are increments of temperature and time, respectively. We calculated average ice nucleation rates ($J = \Delta N_i/\Delta t$) based on the parcel model results from 100 to 600 m and derived the following relationship by a method of trial and error and least squares:

$$J(\mathrm{L}^{-1}\mathrm{s}^{-1}) = \min\left\{a(f_{\mathrm{act}}[\mathrm{dust}])e^{b(273.16-T)}, 2.8w^{2.2}\right\}, \tag{8}$$

where $a = 9.5 \times 10^{-7}$ and $b = 0.443$. The J rate and $\tilde{N}_i$ are associated with dust through the INP surface area calculated with a prescribed initial size distribution, and biases will result for different size distributions. The J rates calculated using Eq. (8) compare very well with the parcel model outputs (Fig. 6). The maximum rates are imposed by the self-limiting effect of dehydration due to ice growth by vapor deposition, which depends on w. A larger w causes more rapid cooling, delaying the effect of dehydration by vapor-to-ice deposition and extending immersion freezing to lower T (and larger J).

So far, we have neglected the effect of pressure on $\tilde{N}_i$ and J. The main effect of P on J is through latent heating: slightly warmer T results from lower P and in turn causes smaller J. In comparison, the effect of P on $\tilde{N}_i$ is much greater as a result of more rapid molecular diffusion and ice growth at lower P (i.e., faster conversion of ice to snow). The ratio of $\tilde{N}_i$ for an initial P of 475 hPa to that of 950 hPa is shown in Fig. 7 as a function of T. The accumulated effect is thus smaller (i.e., larger ratio) when w is larger for a specified cloud thickness. The effect also changes from a mixed-phase regime to a cirrus regime (Fig. 7): the ratios are larger with activated droplets (e.g., $T > 255$ K, for $w = 0.1$ m s^{-1} and [dust] = 2.0 μg m^{-3}) than when condensation ice nucleation prevents activation of liquid droplets (e.g., $T < 252$ K). Figure 8 shows the ratio of $\tilde{N}_i$ at initial P from 475 to 950 hPa to that at 950 hPa (with $w = 0.1$ m s^{-1} and [dust] = 2.0 μg m^{-3}) and averaged for $T > 255$ (mixed phase) and $T < 252$ K (fully glaciated), respectively, versus (P/950 − 1). The linear relationship for the mixed-phase regime is given by

$$\tilde{N}_i(P) = \tilde{N}_i(950)\left[1 + \left(\frac{P}{950} - 1\right)\max(0.3, 1.04 - 1.9w)\right], \tag{9}$$

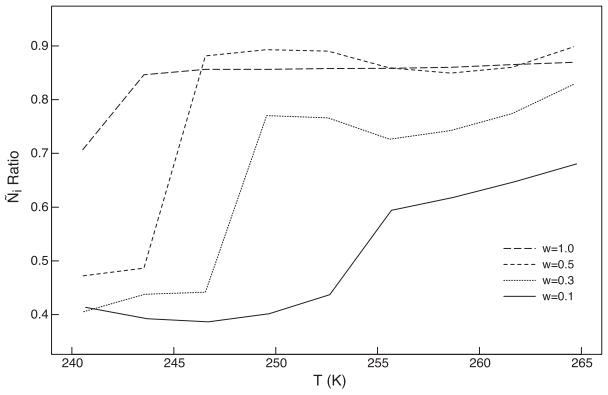

FIG. 7. The ratio of $\tilde{N}_i$ calculated at initial $P = 475$ hPa to $P = 950$ hPa at different T (x axis) and w (solid: 0.1; dotted: 0.3 m s^{-1}; short dash: 0.5 m s^{-1}; and long dash: 1.0 m s^{-1}).

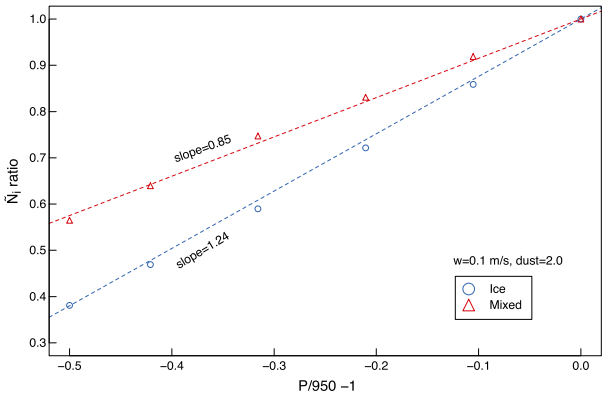

FIG. 8. The ratio of $\tilde{N}_i$ calculated for various initial P to that for 950 hPa vs the ratio (P/950 − 1), with $w = 0.1$ m s^{-1} and [dust] = 2.0 μg m^{-3} specified. The ratios are averaged for ice-only (circles) and mixed-phase (triangles) regimes. The dashed lines are drawn for linear least squares fit.

which also accounts for the dependence on vertical velocity. The variable $\tilde{N}_i(950)$ in Eq. (9) may be calculated based on Eqs. (3) and (4).

6. Comparing model results with observations

The remaining question for this study is whether the parcel model results and thus the parameterization can predict observations in stratus clouds. In Figs. 9 and 10, the parcel model predicted $\tilde{N}_i$ (line) for $w = 0.1$ m s^{-1} and various dust concentrations are compared with aircraft measurements (symbols) of N_i during the Beaufort Arctic Storms Experiment (BASE) and FIRE-ACE campaigns (Gultepe et al. 2001; Rangno and Hobbs 2001; Pinto et al. 2001). Although dust was not measured during the campaigns, concentrations of mineral dust observed at Alert, Ellesmere Island, Nunavut, Canada (82.4°N, 62.3°W), vary with season, ranging from 0.2 μg m^{-3} in February to 0.7 μg m^{-3} in April and about 0.5 μg m^{-3} in autumn (Barrie and Barrie 1990; Fan 2013). Aircraft measurements of supermicron aerosol volume and aerosol calcium were made over the western Arctic in spring 2008 and were used to estimate mineral dust concentrations (McNaughton et al. 2011; Breider et al. 2014; Zwaaftink et al. 2016). The average dust concentrations based on aerosol volume measurements are 0.4 μg m^{-3} below 1 km, increasing to about 3 μg m^{-3} in the middle troposphere (4–8 km) (McNaughton et al. 2011). The average dust concentrations based on aerosol calcium measurements are lower (0.4–2.0 μg m^{-3}) (Breider et al. 2014; Zwaaftink et al. 2016). A vertical velocity of 0.1 m s^{-1} is typical of stratus clouds associated with warm fronts (e.g., Kemppi and Sinclair 2011; Colle et al. 2014).

The measurements of N_i in mixed-phase clouds during the BASE and SHEBA campaigns are shown in Fig. 9. The BASE data are average ice concentrations for each cloud sampled in the altitude range of 1.5–5.5 km (Pinto et al. 2001), where the cloud type is not reported. The SHEBA data are maximum ice concentrations in 1-km pathlengths for altocumulus and stratocumulus clouds (Rangno and Hobbs 2001). A comparison between model results for stratus and observations for stratocumulus is justified based on the similar results from S2 (with $w = 0.1$ m s^{-1}) and S3 simulations (Table 3) but should be interpreted with caution. Maximum concentrations on the order of 0.001 L^{-1} were observed from 260 to 270 K during SHEBA but are not shown in Fig. 9. The observed ice concentrations during BASE and SHEBA are generally between the model lines for a dust concentration of 0.05 μg m^{-3} and for a dust concentration of 2.0 μg m^{-3} at $T < 263$ K (Fig. 9). The BASE data are in better agreement with the model results of $\tilde{N}_i$ for a dust concentration of 0.05, while the SHEBA data are in better agreement for a dust concentration of 0.5 (Fig. 9). It is possible that clear air was present in a flight path, which would lower the average N_i for a cloud during BASE. At $T > 263$ K, the ice crystals are thought to be produced by rime splintering and by shattering of freezing drops (Rangno and Hobbs 2001). These secondary ice production processes are not included in the parcel model.

Three points should be made about these comparisons: First, dust was not measured during BASE and SHEBA; the comparison in Fig. 9 is tentative and intended to guide parameterizations for ice nucleation and the WBF process in large-scale models. However, dust concentrations from 0.05 to 2.0 μg m^{-3} are within the range of observations in the Arctic

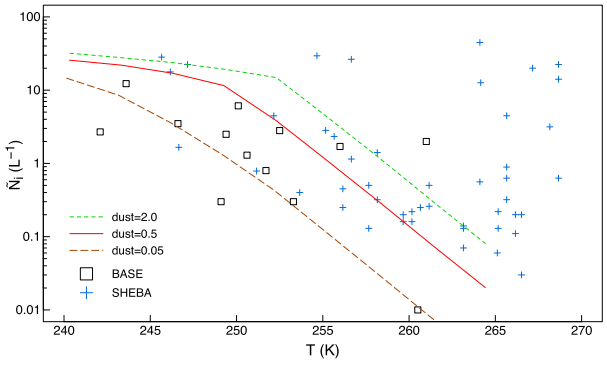

FIG. 9. Number concentration of ice crystals $\tilde{N}_i$ as a function of T in mixed-phase clouds. Black squares indicate observations in mixed-phase clouds (altitude: 1.5–5.5 km) during the BASE field campaign (Pinto et al. 2001), blue crosses indicate observations (maximum in 1-km pathlengths) in liquid-topped altocumulus and stratocumulus during SHEBA (Rangno and Hobbs 2001), and lines indicate model output for specified dust concentrations (see legend for values; $\mu g\,m^{-3}$), $w = 0.1\,m\,s^{-1}$, and initial $P = 950$ hPa. The model simulates immersion freezing based on Alpert and Knopf (2016), with deposition freezing set to zero. Secondary ice production was suggested to occur at $T > 265$ K and possibly at even colder temperatures (Rangno and Hobbs 2001) but is neglected in the parcel model.

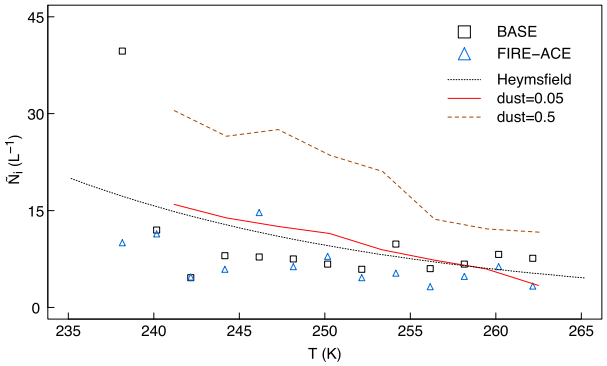

FIG. 10. Number concentration of ice crystals $\tilde{N}_i$ as a function of T in glaciated clouds (i.e., no detectable liquid water). Symbols indicate observations during the BASE (square) and FIRE-ACE (triangle) field campaigns (Gultepe et al. 2001). The dotted line indicates an empirical relation for stratiform cirrus (Heymsfield et al. 2013). The solid and dashed lines indicate model outputs for [dust] = 0.05 and $0.5\,\mu g\,m^{-3}$, respectively, $w = 0.03\,m\,s^{-1}$, and initial $P = 950$ hPa (S4 in Table 3).

(McNaughton et al. 2011; Fan 2013; Breider et al. 2014; Zwaaftink et al. 2016). Lower or higher concentrations of dust are also likely when N_i was measured during BASE and SHEBA. Second, the uncertainty range of ice nucleation rate associated with the ABIFM parameters c and m spans about 2.5 orders of magnitude (Knopf and Alpert 2013; Alpert and Knopf 2016). Larger N_i and J rates are predicted when the model uses the immersion freezing parameterization of Hoose et al. (2010), especially at warmer temperatures (results not shown), which are in better agreement with certain observations [Mixed-Phase Arctic Cloud Experiment (M-PACE) in Table 1]. Third, atmospheric dust may have small ice nucleation efficiency in the immersion mode ($f_{act} \ll 1$). For droplets containing natural dust particles, Kaufmann et al. (2016) report frozen fractions averaged over different dust sources reaching 10% between 244 and 250 K, 25% between 242 and 246 K, and 50% between 239 and 244 K.

The measurements of N_i in glaciated clouds during the BASE and FIRE-ACE (Gultepe et al. 2001) are shown in Fig. 10. An empirical curve derived based on averaged measurements in stratiform cirrus over the Arctic and the midlatitudes (Heymsfield et al. 2013),

$$N_i = 3.1\,e^{0.049(273.16-T)}, \tag{10}$$

is also shown in Fig. 10. The observed ice concentrations are generally about $10\,L^{-1}$ during the campaigns, even at a T of 260 K (Fig. 10). Larger ice numbers were observed at higher altitudes during BASE (Table 1). For instance, a mean N_i of $77.6\,L^{-1}$ was observed in one case during which T was too warm for homogeneous nucleation to have occurred (Table 1). Ice-only clouds may occur through ice nucleation in the deposition mode and in the immersion mode at water subsaturation or in the immersion mode in activated droplets followed by complete droplet evaporation (by the WBF process or by warming).

The parcel model calculates deposition ice nucleation on dry dust particles (S4 simulations in Table 3). It reproduces the observed N_i with [dust] = $0.05\,\mu g\,m^{-3}$ and $w = 0.03\,m\,s^{-1}$ and overpredicts with [dust] = $0.5\,\mu g\,m^{-3}$ (Fig. 10). A dust concentration of $0.05\,\mu g\,m^{-3}$ is 2%–10% of the amount observed in spring 2008 (McNaughton et al. 2011; Breider et al. 2014). The parcel model specifies a θ of 12.7° for deposition nucleation on dust particles of all sizes (Hoose et al. 2010), corresponding to an onset SSi between 11% (at ~260 K) and 14% (~240 K). This may suggest active fractions of 2%–10% for the range of SSi values (11%–14%). Previously, it was observed that at $T = 240$ K, the INP at −8% SSw (i.e., deposition ice nucleation at SSi = 13%) is only 1% of the INP at 5% SSw (immersion freezing) in the dust-laden Saharan air layer (Boose et al. 2016). Similarly low active fractions in the deposition mode relative to that in the immersion mode were observed in laboratory ice nucleation experiments using Arizona Test Dust, K-feldspar, illite, montmorillonite, and quartz particles (Kulkarni et al. 2014). For all these particles, the active fraction in the deposition mode increases with SSi (Kulkarni et al. 2014).

The onset RH of ice formation via deposition nucleation on mineral dust was observed to decrease with particle size (Archuleta et al. 2005; Kanji and Abbatt 2010; Koehler et al. 2010) and with total particulate surface area (Kanji et al. 2008). As the onset SSi increases with contact angle θ, expected by CNT (Hoose et al. 2010; Kanji and Abbatt 2010; Wang and Knopf 2011), this may indicate a dependence of θ on particle size or total available INP surface area, which is neglected in the parcel model. Supermicron particles are few but account for most of the dust mass observed in the atmosphere and would also contribute significantly to total particle surface area. Submicron dust particles are more numerous but are poor INPs in the deposition mode at $T > 243$ K (Hoose and Möhler 2012), which is consistent with a large θ and high onset SSi for these particles. The parcel model has likely overestimated N_i if θ is larger than 12.7° for some submicron particles and decreases with the size as shown by the laboratory experiments. The parcel model could be improved by prescribing a probability distribution function for θ based on measurements (Niedermeier et al. 2014; Wang and Liu 2014; Wang et al. 2014).

The parcel model may also overestimate N_i by neglecting the effect of soluble coating. The ice nucleating ability of desert dust particles may be decreased by coating of nitric and sulfuric acids, ammonium nitrate, and sulfate (Möhler et al. 2008; Cziczo et al. 2009; Eastwood et al. 2009; Chernoff and Bertram 2010; Sullivan et al. 2010; Niedermeier et al. 2011; Reitz et al. 2011; Kulkarni et al. 2014). A study of aerosol aging in a global tracer transport model suggests that a large fraction of dust particles in the Arctic is coated by nitrate and sulfate (unpublished result), while soluble coating during atmospheric transport is not significant in the Saharan air layer over the tropical North Atlantic Ocean (Fan et al. 2004). On the contrary, Saharan dust particles were found to nucleate droplets in eastern Atlantic clouds (Twohy et al. 2009), suggesting that a significant fraction of the particles are hygroscopic and likely coated with soluble materials. Measurements of the size distribution and chemical and mineral composition of ice evaporation residuals would provide useful information on the causes of low active fraction in the deposition mode and cloud glaciation at relatively warm temperatures.

In Fig. 11, we compare the J rates calculated by Eq. (8) and by Eqs. (5), (6a), and (7). Again, the comparisons are only tentative because of a lack of concurrent dust and INP measurements. The J rates based on Meyers et al. (1992) straddle the model results for the range of dust concentrations (0.05–10 μg m^{-3}), in better agreement at low dust–low T and at higher dust–higher T,

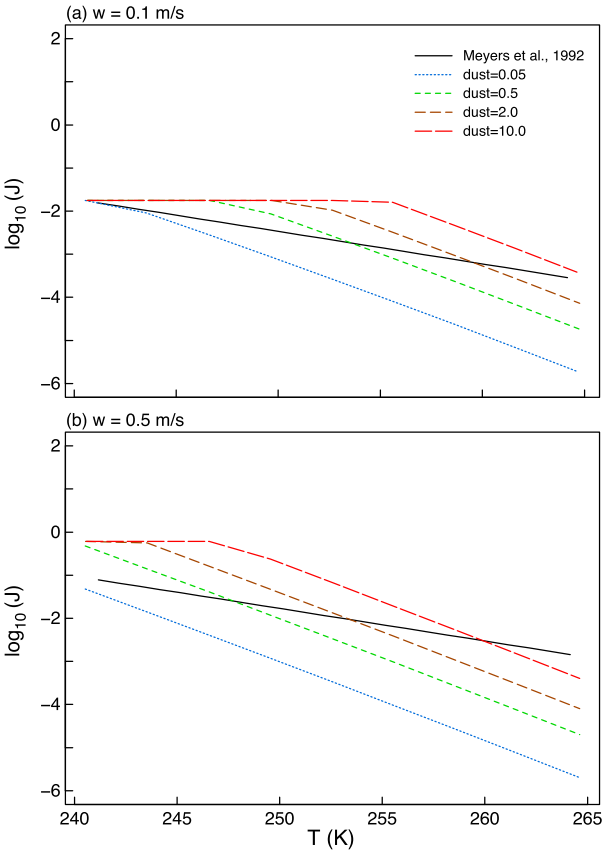

FIG. 11. The rate of ice nucleation J ($L^{-1}s^{-1}$, shown in $\log_{10}$) as a function of T for w = (a) 0.1 and (b) 0.5 m s^{-1}. Solid line indicates calculations based on the empirical relation of Meyers et al. (1992), using Eqs. (5), (6a), and (7). Dashed lines indicate calculations based on Eq. (8) for two w values and four dust concentrations (blue: 0.05 μg m^{-3}; green: 0.5 μg m^{-3}; brown: 2.0 μg m^{-3}; and red: 10 μg m^{-3}).

respectively. At $w = 0.1$ m s^{-1}, the J rates calculated by Eqs. (5), (6a), and (7) are within that calculated by Eq. (8) for the range of dust concentrations (Fig. 11a). The differences between them can be as large as one to two orders of magnitude. At $w = 0.5$ m s^{-1}, larger J rates are predicted by both and the differences between them are also greater (Fig. 11b).

In Fig. 12, we compare the J rates calculated by Eq. (8) and by Eqs. (5), (6b), and (7). The dust number concentrations ($n_{a>0.5\mu m}$ = 0.017, 0.17, 0.68, and 3.4 cm^{-3} for dust concentrations of 0.05, 0.5, 2.0, and 10 μg m^{-3}, respectively) are estimated based on a prescribed size distribution. The J rates based on DeMott et al. (2015) show similar temperature dependence with those based on parcel model calculations, as suggested by the nearly parallel trends in Fig. 12. The coefficient for the exponential T dependence is 0.443 in Eq. (8) for the parcel model and 0.46 in Eq. (6b) for the empirical relation of DeMott et al. (2015). However, the J rates based on DeMott et al. (2015) are lower than the parcel

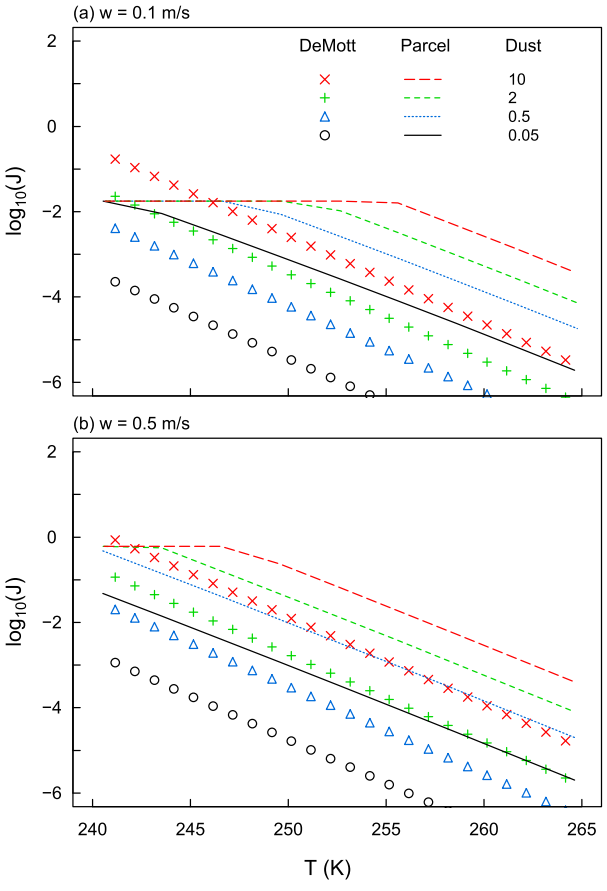

FIG. 12. The rate of ice nucleation J ($L^{-1}s^{-1}$, shown in $\log_{10}$) as a function of T for w = (a) 0.1 and (b) 0.5 m s^{-1}. Symbols indicate calculations based on the empirical relation of DeMott et al. (2015), using Eqs. (5), (6b), and (7), with $n_{a>0.5\mu m}$ = 0.017, 0.17, 0.68, and 3.4 cm^{-3} for [dust] = 0.05, 0.5, 2.0, and 10 $\mu g\, m^{-3}$, respectively. Lines indicate calculations based on Eq. (8) for two w values and four dust concentrations (black: 0.05 $\mu g\, m^{-3}$; blue: 0.5 $\mu g\, m^{-3}$; green: 2.0 $\mu g\, m^{-3}$; and red: 10 $\mu g\, m^{-3}$).

model by about two orders of magnitude. The difference may be attributed partly to a lack of time dependence for nucleation in the empirical relation, which was derived based on continuous flow diffusion chamber (CFDC) measurements. The residence time of air in a CFDC is typically 10 s (DeMott et al. 2015), much shorter than in a stratus cloud. The parcel model assumes f_{act} = 1 for immersion freezing with dust particles, which may also contribute to the differences shown in Fig. 12. Laboratory measurements have shown that not all dust particles are active INPs in the temperature range for mixed-phase clouds (e.g., Kulkarni et al. 2014).

7. Summary

In this study, we carried out parcel model simulations of the WBF process in mixed-phase clouds. Two parameterizations of ice nucleation based on laboratory experiments were used in separate simulations. The air parcel was assumed to oscillate in a horizontal layer for a stratocumulus cloud, undergo ascent at a constant vertical velocity for a stratus cloud, or oscillate in a slanted layer. The model results for typical aerosol concentrations observed in the Arctic were compared to aircraft measurements of ice crystals. However, the comparison is tentative and intended to guide parameterizations. More rigorous comparison is only possible if measurements will be made concurrently of ice crystals, vertical air velocities, and insoluble aerosols in the future. It is useful to obtain characterizations of ice crystal evaporation residues including their size distribution and chemical and mineralogical compositions.

The model results show rapid changes in ice nucleation, ice number, relative humidity, and ice–liquid partition within a 500-m vertical distance. Because these fast processes are not readily resolved in large-scale atmospheric models, parameterizations were constructed in this study for ice in mixed-phase clouds based on the parcel model results. The parameterizations for J and $\tilde{N}_i$ developed in this study allow INP to vary with dust and vertical velocity in addition to temperature, represent a time-integrated effect of the WBF process in ~500-m cloud layers, and could be used provisionally in climate models to improve the simulation of mixed-phase clouds.

Acknowledgments. The authors are grateful to three anonymous reviewers for comments that led to significant improvement of the manuscript. Catherine Raphael helped with improving the graphs. Huan Guo and Paul Ginoux commented on a draft of the manuscript. D. K. acknowledges support by the U.S. Department of Energy, Office of Science (BER), under Award DE-SC0016370.

REFERENCES

Alpert, P. A., and D. A. Knopf, 2016: Analysis of isothermal and cooling-rate-dependent immersion freezing by a unifying stochastic ice nucleation model. *Atmos. Chem. Phys.*, **16**, 2083–2107, doi:10.5194/acp-16-2083-2016.

——, J. Y. Aller, and D. A. Knopf, 2011: Ice nucleation from aqueous NaCl droplets with and without marine diatoms. *Atmos. Chem. Phys.*, **11**, 5539–5555, doi:10.5194/acp-11-5539-2011.

Archuleta, C. M., P. J. DeMott, and S. M. Kreidenweis, 2005: Ice nucleation by surrogates for atmospheric mineral dust and mineral dust/sulfate particles at cirrus temperatures. *Atmos. Chem. Phys.*, **5**, 2617–2634, doi:10.5194/acp-5-2617-2005.

Avramov, A., and Coauthors, 2011: Towards ice formation closure in Arctic mixed-phase boundary layer clouds during ISDAC. *J. Geophys. Res.*, **116**, D00T08, doi:10.1029/2011JD015910.

Barahona, D., J. Rodriguez, and A. Nenes, 2010: Sensitivity of the global distribution of cirrus ice crystal concentration to heterogeneous freezing. *J. Geophys. Res.*, **115**, D23213, doi:10.1029/2010JD014273.

Barrie, L. A., and M. J. Barrie, 1990: Chemical components of lower tropospheric aerosols in the high Arctic: Six years of observations. *J. Atmos. Chem.*, **11**, 211–226, doi:10.1007/BF00118349.

Boose, Y., and Coauthors, 2016: Ice nucleation particles in the Saharan air layer. *Atmos. Chem. Phys.*, **16**, 9067–9087, doi:10.5194/acp-16-9067-2016.

Breider, T. J., L. J. Mickley, D. J. Jacob, Q. Wang, J. A. Fisher, R. Y.-W. Chang, and B. Alexander, 2014: Annual distributions and sources of Arctic aerosol components, aerosol optical depth, and aerosol absorption. *J. Geophys. Res. Atmos.*, **119**, 4107–4124, https://doi.org/10.1002/2013JD020996.

Bullard, J. E., and Coauthors, 2016: High-latitude dust in the Earth system. *Rev. Geophys.*, **54**, 447–485, doi:10.1002/2016RG000518.

Cesana, G., J. E. Kay, H. Chepfer, J. M. English, and G. de Boer, 2012: Ubiquitous low-level liquid-containing Arctic clouds: New observations and climate model constraints from CALIPSO-GOCCP. *Geophys. Res. Lett.*, **39**, L20804, https://doi.org/10.1029/2012GL053385.

Chen, J.-P., A. Hazra, and Z. Levin, 2008: Parameterizing ice nucleation rates using contact angle and activation energy derived from laboratory data. *Atmos. Chem. Phys.*, **8**, 7431–7449, doi:10.5194/acp-8-7431-2008.

Chernoff, D. I., and A. K. Bertram, 2010: Effects of sulfate coatings on the ice nucleation properties of a biological ice nucleus and several types of minerals. *J. Geophys. Res.*, **115**, D20205, doi:10.1029/2010JD014254.

Colle, B. A., D. Stark, and S. E. Yuter, 2014: Surface microphysical observations within East Coast winter storms on Long Island, New York. *Mon. Wea. Rev.*, **142**, 3126–3146, doi:10.1175/MWR-D-14-00035.1.

Crusius, J., A. W. Schroth, S. Gassó, C. M. Moy, R. C. Levy, and M. Gatica, 2011: Glacial flour dust storms in the Gulf of Alaska: Hydrologic and meteorological controls and their importance as a source of bioavailable iron. *Geophys. Res. Lett.*, **38**, L06602, doi:10.1029/2010GL046573.

Curry, J. A., and G. F. Herman, 1985: Infrared radiative properties of summertime Arctic stratus clouds. *J. Climate Appl. Meteor.*, **24**, 525–538, doi:10.1175/1520-0450(1985)024<0525:IRPOSA>2.0.CO;2.

——, W. B. Rossow, D. Randall, and J. L. Schramm, 1996: Overview of Arctic cloud and radiation properties. *J. Climate*, **9**, 1731–1764, doi:10.1175/1520-0442(1996)009<1731:OOACAR>2.0.CO;2.

Cziczo, D. J., K. D. Froyd, S. J. Gallavardin, O. Moehler, S. Benz, H. Saathoff, and D. M. Murphy, 2009: Deactivation of ice nuclei due to atmospherically relevant surface coatings. *Environ. Res. Lett.*, **4**, 044013, doi:10.1088/1748-9326/4/4/044013.

de Boer, G., T. Hashino, and G. J. Tripoli, 2010: Ice nucleation through immersion freezing in mixed-phase stratiform clouds: Theory and numerical simulations. *Atmos. Res.*, **96**, 315–324, doi:10.1016/j.atmosres.2009.09.012.

——, H. Morrison, M. D. Shupe, and R. Hildner, 2011: Evidence of liquid dependent ice nucleation in high-latitude stratiform clouds from surface remote sensors. *Geophys. Res. Lett.*, **38**, L01803, doi:10.1029/2010GL046016.

DeMott, P. J., and Coauthors, 2010: Predicting global atmospheric ice nuclei distributions and their impacts on climate. *Proc. Natl. Acad. Sci. USA*, **107**, 11 217–11 222, doi:10.1073/pnas.0910818107.

——, and Coauthors, 2015: Integrating laboratory and field data to quantify the immersion freezing ice nucleation activity of mineral dust particles. *Atmos. Chem. Phys.*, **15**, 393–409, doi:10.5194/acp-15-393-2015.

——, and Coauthors, 2016: Sea spray aerosol as a unique source of ice nucleating particles. *Proc. Natl. Acad. Sci. USA*, **113**, 5797–5803, doi:10.1073/pnas.1514034112.

Eastwood, M. L., S. Cremel, M. Wheeler, B. J. Murray, E. Girard, and A. K. Bertram, 2009: Effects of sulfuric acid and ammonium sulfate coatings on the ice nucleation properties of kaolinite particles. *Geophys. Res. Lett.*, **36**, L02811, doi:10.1029/2008GL035997.

Fan, J., S. J. Ghan, M. Ovchinnikov, X. Liu, P. R. Rasch, and A. Korolev, 2011: Representation of Arctic mixed-phase clouds and Wegener-Bergeron-Findeisen process in climate models: Perspectives from a cloud-resolving study. *J. Geophys. Res.*, **116**, D00T07, doi:10.1029/2010JD015375.

Fan, S.-M., 2013: Modeling of observed mineral dust aerosols in the Arctic and the impact on winter season low-level clouds. *J. Geophys. Res. Atmos.*, **118**, 11 161–11 174, doi:10.1002/jgrd.50842.

——, L. W. Horowitz, H. Levy II, and W. J. Moxim, 2004: Impact of air pollution on wet deposition of mineral dust aerosols. *Geophys. Res. Lett.*, **31**, L02104, doi:10.1029/2003GL018501.

Fletcher, N. H., 1962: *The Physics of Rainclouds*. Cambridge University Press, 390 pp.

Fridlind, A. M., B. van Diedenhoven, A. S. Ackerman, A. Avramov, A. Mrowiec, H. Morrison, P. Zuidema, and M. D. Shupe, 2012: A FIRE-ACE/SHEBA case study of mixed-phase Arctic boundary layer clouds: Entrainment rate limitations on rapid primary ice nucleation processes. *J. Atmos. Sci.*, **69**, 365–389, doi:10.1175/JAS-D-11-052.1.

Friedman, B., G. Kulkarni, J. Beránek, A. Zelenyuk, J. Thornton, and D. Cziczo, 2011: Ice nucleation and droplet formation by bare and coated soot particles. *J. Geophys. Res.*, **116**, D17203, doi:10.1029/2011JD015999.

Gayet, J.-F., R. Treffeisen, A. Helbig, J. Bareiss, A. Matsuki, A. Herber, and A. Schwarzenboeck, 2009: On the onset of the ice phase in boundary layer Arctic clouds. *J. Geophys. Res.*, **114**, D19201, doi:10.1029/2008JD011348.

Gultepe, I., G. A. Isaac, and S. G. Cober, 2001: Ice crystal number concentration versus temperature for climate studies. *Int. J. Climatol.*, **21**, 1281–1302, doi:10.1002/joc.642.

Hallett, J., and S. C. Mossop, 1974: Production of secondary ice particles during the riming process. *Nature*, **249**, 26–28, doi:10.1038/249026a0.

Heymsfield, A. J., C. Schmitt, and A. Bansemer, 2013: Ice cloud particle size distributions and pressure-dependent terminal velocities from in situ observations at temperatures from 0° to −86°C. *J. Atmos. Sci.*, **70**, 4123–4154, doi:10.1175/JAS-D-12-0124.1.

Hoose, C., and O. Möhler, 2012: Heterogeneous ice nucleation on atmospheric aerosols: A review of results from laboratory experiments. *Atmos. Chem. Phys.*, **12**, 9817–9854, doi:10.5194/acp-12-9817-2012.

——, J. E. Kristjánsson, J.-P. Chen, and A. Hazra, 2010: A classical theory-based parameterization of heterogeneous ice nucleation by mineral dust, soot, and biological particles in a global climate model. *J. Atmos. Sci.*, **67**, 2483–2503, doi:10.1175/2010JAS3425.1.

Jiang, H., W. R. Cotton, J. O. Pinto, J. A. Curry, and M. J. Weissbluth, 2000: Cloud resolving simulations of mixed-phase Arctic stratus observed during BASE: Sensitivity to

concentration of ice crystals and large-scale heat and moisture advection. *J. Atmos. Sci.*, **57**, 2105–2117, doi:10.1175/1520-0469(2000)057<2105:CRSOMP>2.0.CO;2.

Kanji, Z. A., and J. P. D. Abbatt, 2010: Ice nucleation onto Arizona test dust at cirrus temperatures: Effect of temperature and aerosol size on onset relative humidity. *J. Phys. Chem.*, **114A**, 935–941, doi:10.1021/jp908661m.

——, F. Octavian, and J. P. D. Abbatt, 2008: Ice formation via deposition nucleation on mineral dust and organics: Dependence of onset relative humidity on total particulate surface area. *Environ. Res. Lett.*, **3**, 025004, https://doi.org/10.1088/1748-9326/3/2/025004.

Kaufmann, L., C. Marcolli, J. Hofer, V. Pinti, C. R. Hoyle, and T. Peter, 2016: Ice nucleation efficiency of natural dust samples in the immersion mode. *Atmos. Chem. Phys.*, **16**, 11 177–11 206, doi:10.5194/acp-16-11177-2016.

Kemppi, M. L., and V. A. Sinclair, 2011: Structure of a warm front: Helsinki testbed observations and model simulation. *Mon. Wea. Rev.*, **139**, 2876–2900, doi:10.1175/MWR-D-10-05003.1.

Khvorostyanov, V. I., and J. A. Curry, 2004: The theory of ice nucleation by heterogeneous freezing of deliquescent mixed CCN. Part I: Critical radius, energy, and nucleation rates. *J. Atmos. Sci.*, **61**, 2676–2691, doi:10.1175/JAS3266.1.

Klein, S. A., and Coauthors, 2009: Intercomparison of model simulations of mixed-phase clouds observed during the ARM Mixed-Phase Arctic Cloud Experiment. I: Single-layer cloud. *Quart. J. Roy. Meteor. Soc.*, **135**, 979–1002, doi:10.1002/qj.416.

Knopf, D. A., and P. A. Alpert, 2013: A water activity based model of heterogeneous ice nucleation kinetics for freezing of water and aqueous solution droplets. *Faraday Discuss.*, **165**, 513–534, doi:10.1039/c3fd00035d.

——, ——, B. Wang, and J. Y. Aller, 2011: Stimulation of ice nucleation by marine diatoms. *Nat. Geosci.*, **4**, 88–90, doi:10.1038/ngeo1037.

Koehler, K. A., S. M. Kreidenweis, P. J. DeMott, M. D. Petters, A. J. Prenni, and O. Möhler, 2010: Laboratory investigations of the impact of mineral dust aerosol on cold cloud formation. *Atmos. Chem. Phys.*, **10**, 11 955–11 968, doi:10.5194/acp-10-11955-2010.

Koop, T., and B. Zobrist, 2009: Parameterizations for ice nucleation in biological and atmospheric systems. *Phys. Chem. Chem. Phys.*, **11**, 10 839–10 850, doi:10.1039/b914289d.

——, B. Luo, A. Tsias, and T. Peter, 2000: Water activity as the determinant for homogeneous ice nucleation in aqueous solutions. *Nature*, **406**, 611–614, doi:10.1038/35020537.

Kulkarni, G., C. Sanders, K. Zhang, X. Liu, and C. Zhao, 2014: Ice nucleation of bare and sulfuric acid-coated mineral dust particles and implication for cloud properties. *J. Geophys. Res. Atmos.*, **119**, 9993–10 011, https://doi.org/10.1002/2014JD021567.

Lawson, R. P., S. Woods, and H. Morrison, 2015: The microphysics of ice and precipitation development in tropical cumulus clouds. *J. Atmos. Sci.*, **72**, 2429–2445, doi:10.1175/JAS-D-14-0274.1.

Liu, X., and J. E. Penner, 2005: Ice nucleation parameterization for global models. *Meteor. Z.*, **14**, 499–514, doi:10.1127/0941-2948/2005/0059.

——, and Coauthors, 2011: Testing cloud microphysics parameterizations in NCAR CAM5 with ISDAC and M-PACE observations. *J. Geophys. Res.*, **116**, D00T11, https://doi.org/10.1029/2011JD015889.

Lloyd, G., and Coauthors, 2015: Observations and comparisons of cloud microphysical properties in spring and summertime Arctic stratocumulus clouds during the ACCACIA campaign. *Atmos. Chem. Phys.*, **15**, 3719–3737, https://doi.org/10.5194/acp-15-3719-2015.

McFarquhar, G. M., G. Zhang, M. R. Poellot, G. L. Kok, R. McCoy, T. Tooman, A. Fridlind, and A. J. Heymsfield, 2007: Ice properties of single-layer stratocumulus during the Mixed-Phase Arctic Cloud Experiment: 1. Observations. *J. Geophys. Res.*, **112**, D24201, doi:10.1029/2007JD008633.

——, and Coauthors, 2011: Indirect and Semi-Direct Aerosol Campaign (ISDAC): The impact of Arctic aerosols on clouds. *Bull. Amer. Meteor. Soc.*, **92**, 183–201, doi:10.1175/2010BAMS2935.1.

McNaughton, C. S., and Coauthors, 2011: Absorbing aerosol in the troposphere of the western Arctic during the 2008 ARCTAS/ARCPAC airborne field campaigns. *Atmos. Chem. Phys.*, **11**, 7561–7582, doi:10.5194/acp-11-7561-2011.

Meyers, M. P., P. J. DeMott, and W. R. Cotton, 1992: New primary ice-nucleation parameterizations in an explicit cloud model. *J. Appl. Meteor.*, **31**, 708–721, doi:10.1175/1520-0450(1992)031<0708:NPINPI>2.0.CO;2.

Möhler, O., and Coauthors, 2008: The effect of organic coating on the heterogeneous ice nucleation efficiency of mineral dust aerosols. *Environ. Res. Lett.*, **3**, 025007, doi:10.1088/1748-9326/3/2/025007.

Morrison, H., and A. Gettelman, 2008: A new two-moment bulk stratiform cloud microphysics scheme in the Community Atmosphere Model, version 3 (CAM3). Part I: Description and numerical tests. *J. Climate*, **21**, 3642–3659, doi:10.1175/2008JCLI2105.1.

——, and Coauthors, 2009: Intercomparison of model simulations of mixed-phase clouds observed during the ARM Mixed-Phase Arctic Cloud Experiment. II: Multi-layered cloud. *Quart. J. Roy. Meteor. Soc.*, **135**, 1003–1019, doi:10.1002/qj.415.

——, G. de Boer, G. Feingold, J. Harrington, M. D. Shupe, and K. Sulia, 2012: Resilience of persistent Arctic mixed-phase clouds. *Nat. Geosci.*, **5**, 11–17, doi:10.1038/ngeo1332.

Murray, B. J., D. O'Sullivan, J. D. Atkinson, and M. E. Webb, 2012: Ice nucleation by particles immersed in supercooled cloud droplets. *Chem. Soc. Rev.*, **41**, 6519–6554, doi:10.1039/c2cs35200a.

Niedermeier, D., and Coauthors, 2011: Experimental study of the role of physicochemical surface processing on the IN ability of mineral dust particles. *Atmos. Chem. Phys.*, **11**, 11 131–11 144, doi:10.5194/acp-11-11131-2011.

——, B. Ervens, T. Clauss, J. Voigtländer, H. Wex, S. Hartmann, and F. Stratmann, 2014: A computationally efficient description of heterogeneous freezing: A simplified version of the soccer ball model. *Geophys. Res. Lett.*, **41**, 736–741, doi:10.1002/2013GL058684.

Niemand, M., and Coauthors, 2012: A particle-surface-area-based parameterization of immersion freezing on desert dust particles. *J. Atmos. Sci.*, **69**, 3077–3092, doi:10.1175/JAS-D-11-0249.1.

Noer, G., Ø. Saetra, T. Lien, and Y. Gusdal, 2011: A climatological study of polar lows in the Nordic seas. *Quart. J. Roy. Meteor. Soc.*, **137**, 1762–1772, doi:10.1002/qj.846.

Phillips, V. T. J., P. J. DeMott, and C. Andronache, 2008: An empirical parameterization of heterogeneous ice nucleation for multiple chemical species of aerosol. *J. Atmos. Sci.*, **65**, 2757–2783, doi:10.1175/2007JAS2546.1.

——, ——, ——, K. A. Pratt, K. A. Prather, R. Subramanian, and C. Twohy, 2013: Improvements to an empirical parameterization of heterogeneous ice nucleation and its comparison with observations. *J. Atmos. Sci.*, **70**, 378–409, doi:10.1175/JAS-D-12-080.1.

Pinto, J. O., J. A. Curry, and J. M. Intrieri, 2001: Cloud-aerosol interactions during autumn over Beaufort Sea. *J. Geophys. Res.*, **106**, 15 077–15 097, doi:10.1029/2000JD900267.

Prenni, A. J., P. J. DeMott, D. C. Rogers, S. M. Kreidenweis, G. M. McFarquhar, G. Zhang, and M. D. Poellot, 2009: Ice nuclei characteristics from M-PACE and their relation to ice formation in clouds. *Tellus*, **61B**, 436–448, https://doi.org/10.1111/j.1600-0889.2009.00415.x.

Pruppacher, H. R., and J. D. Klett, 1997: *Microphysics of Clouds and Precipitation*. Kluwer Academic Publishers, 954 pp.

Rangno, A. L., 2008: Fragmentation of freezing drops in shallow maritime frontal clouds. *J. Atmos. Sci.*, **65**, 1455–1466, doi:10.1175/2007JAS2295.1.

——, and P. V. Hobbs, 2001: Ice particles in stratiform clouds in the Arctic and possible mechanisms for the production of high ice concentrations. *J. Geophys. Res.*, **106**, 15 065–15 075, doi:10.1029/2000JD900286.

Reitz, P., and Coauthors, 2011: Surface modification of mineral dust particles by sulfuric acid processing: Implications for ice nucleation abilities. *Atmos. Chem. Phys.*, **11**, 7839–7858, doi:10.5194/acp-11-7839-2011.

Rotstayn, L. D., B. F. Ryan, and J. J. Katzfey, 2000: A scheme for calculation of the liquid fraction in mixed-phase stratiform clouds in large-scale models. *Mon. Wea. Rev.*, **128**, 1070–1088, doi:10.1175/1520-0493(2000)128<1070:ASFCOT>2.0.CO;2.

Shupe, M. D., 2011: Clouds at Arctic atmospheric observatories. Part II: Thermodynamic phase characteristics. *J. Appl. Meteor. Climatol.*, **50**, 645–661, doi:10.1175/2010JAMC2468.1.

——, S. Y. Matrosov, and T. Uttal, 2006: Arctic mixed-phase cloud properties derived from surface-based sensors at SHEBA. *J. Atmos. Sci.*, **63**, 697–711, https://doi.org/10.1175/JAS3659.1.

Solomon, A., M. D. Shupe, P. O. G. Persson, and H. Morrison, 2011: Moisture and dynamical interactions maintaining decoupled Arctic mixed-phase stratocumulus in the presence of a humidity inversion. *Atmos. Chem. Phys.*, **11**, 10 127–10 148, doi:10.5194/acp-11-10127-2011.

Sotiropoulou, G., J. Sedlar, R. Forbes, and M. Tjernström, 2016: Summer Arctic clouds in the ECMWF forecast model: An evaluation of cloud parameterization schemes. *Quart. J. Roy. Meteor. Soc.*, **142**, 387–400, doi:10.1002/qj.2658.

Sulia, K. J., and J. Y. Harrington, 2011: Ice aspect ratio influences on mixed-phase clouds: Impacts on phase transitioning in parcel models. *J. Geophys. Res.*, **116**, D21309, doi:10.1029/2011JD016298.

Sullivan, R. C., and Coauthors, 2010: Irreversible loss of ice nucleation active sites in mineral dust particles caused by sulphuric acid condensation. *Atmos. Chem. Phys.*, **10**, 11 471–11 487, doi:10.5194/acp-10-11471-2010.

Tan, I., T. Storelvmo, and M. D. Zelinka, 2016: Observational constraints on mixed-phase clouds imply higher climate sensitivity. *Science*, **352**, 224–227, doi:10.1126/science.aad5300.

Tobo, Y., and Coauthors, 2013: Biological aerosol particles as a key determinant of ice nuclei populations in a forest ecosystem. *J. Geophys. Res. Atmos.*, **118**, 10 100–10 110, https://doi.org/10.1002/jgrd.50801.

Twohy, C. H., and Coauthors, 2009: Saharan dust particles nucleate droplets in eastern Atlantic clouds. *Geophys. Res. Lett.*, **36**, L01807, doi:10.1029/2008GL035846.

Verlinde, J., and Coauthors, 2007: The Mixed-Phase Arctic Cloud Experiment. *Bull. Amer. Meteor. Soc.*, **88**, 205–221, doi:10.1175/BAMS-88-2-205.

Wang, B., and D. A. Knopf, 2011: Heterogeneous ice nucleation on particles composed of humic-like substances impacted by O_3. *J. Geophys. Res.*, **116**, D03205, https://doi.org/10.1029/2010JD014964.

Wang, Y., and X. Liu, 2014: Immersion freezing by natural dust based on a soccer ball model with the Community Atmospheric Model version 5: Climate effects. *Environ. Res. Lett.*, **9**, 124020, doi:10.1088/1748-9326/9/12/124020.

——, ——, C. Hoose, and B. Wang, 2014: Different contact angle distributions for heterogeneous ice nucleation in the Community Atmospheric Model version 5. *Atmos. Chem. Phys.*, **14**, 10 411–10 430, doi:10.5194/acp-14-10411-2014.

Westbrook, C. D., and A. J. Illingworth, 2013: The formation of ice in a long-lived supercooled layer cloud. *Quart. J. Roy. Meteor. Soc.*, **139**, 2209–2221, doi:10.1002/qj.2096.

Wilson, T. W., and Coauthors, 2015: A marine biogenic source of atmospheric ice-nucleating particles. *Nature*, **525**, 234–238, doi:10.1038/nature14986.

Xie, S., J. Boyle, S. A. Klein, X. Liu, and S. Ghan, 2008: Simulations of Arctic mixed-phase clouds in forecasts with CAM3 and AM2 for M-PACE. *J. Geophys. Res.*, **113**, D04211, https://doi.org/10.1029/2007JD009225.

Yang, F., M. Ovchinnikov, and R. A. Shaw, 2013: Minimalist model of ice microphysics in mixed-phase stratiform clouds. *Geophys. Res. Lett.*, **40**, 3756–3760, doi:10.1002/grl.50700.

——, ——, and ——, 2014: Microphysical consequences of the spatial distribution of ice nucleation in mixed-phase stratiform clouds. *Geophys. Res. Lett.*, **41**, 5280–5287, doi:10.1002/2014GL060657.

Yun, Y., and J. E. Penner, 2013: An evaluation of the potential radiative forcing and climatic impact of marine organic aerosols as heterogeneous ice nuclei. *Geophys. Res. Lett.*, **40**, 4121–4126, doi:10.1002/grl.50794.

Zimmermann, F., S. Weinbruch, L. Schütz, H. Hofmann, M. Ebert, K. Kandler, and A. Worringen, 2008: Ice nucleation properties of the most abundant mineral dust phases. *J. Geophys. Res.*, **113**, D23204, doi:10.1029/2008JD010655.

Zobrist, B., T. Koop, B. Luo, C. Marcolli, and T. Peter, 2007: Heterogeneous ice nucleation rate coefficient of water droplets coated by a nonadecanol monolayer. *J. Phys. Chem.*, **111C**, 2149–2155, https://doi.org/10.1021/jp066080w.

Zwaaftink, C. D., H. Grythe, H. Skov, and A. Stohl, 2016: Substantial contribution of northern high-latitude sources to mineral dust in the Arctic. *J. Geophys. Res. Atmos.*, **121**, 13 678–13 697, https://doi.org/10.1002/2016JD025482.